Modular Two-Degree-of-Freedom Transformable Wheels Capable of Overcoming Obstacle

Yunhyuk Lee, Sijun Ryu, Jee Ho Won, SangGyun Kim, Hwa Soo Kim, *Member, IEEE*, and TaeWon Seo, *Senior Member, IEEE*

***Abstract*—This study presents modular transformable wheels capable of overcoming obstacles. They can be used for indoor service robots or service platforms such as wheelchairs and baby carriages, which often move up and down on thresholds or on sidewalks. The structure of the wheel and transformation mechanism are introduced. The wheel has two built-in brushless DC (BLDC) motors. The BLDC motor is remodeled to add the gear box inside. These motors create a two-degree-of-freedom (2-DOF) transformation of the wheel. The 2-DOF mechanism is achieved by a 7-bar linkage with six rotational joints and one prismatic joint. A platform using the presented modular transformable wheels was used to experimentally verify the ability to climb up and down a staircase.**

***Index Terms*—Mobile platform, modular wheel, overcoming obstacle, service robot, transformable wheel.**

I. Introduction

SERVICE robots and platforms often use wheels as driving methods. This is because wheels provide the most effective and fastest means to navigate on flat surfaces. LG AirStar, Starship, Double 2, wheelchairs, and baby carriages are examples of service robots and platforms for guidance, delivery, and telepresence, which use wheels for movement to a destination [1]–[3]. However, it is difficult for wheels to perform effectively when they come across obstacles with different heights, such as thresholds and sidewalks. It is not possible for a wheel to overcome obstacles that are higher than half of its diameter. Therefore, the ability to overcome obstacles is necessary for service robots and platforms.

The two-legged robots were also studied [4]–[7]. The legged mechanism also excels at climbing stairs and other terrain. However, it is hard to control, and many strategies are needed to overcome the obstacles. On the other hand, the efficiency and stability of a conventional wheel is better than legged mechanism at a flat surface. A previous research presented wheels that could overcome obstacles by combining the wheels with linkages. Platforms using wheel-linkage mechanisms referred to as rocker-bogie are SHRIMP and CRAB [8], [9]. The rocker-bogie mechanism is useful to overcome obstacles of various heights and has high stability while climbing obstacles. This mechanism causes the wheel to roll up the vertical plane of the obstacle and moves it upwards; moreover, it has a low overcoming speed. Therefore, it is impossible to overcome an obstacle in the absence of a vertical plane or stair nose. Because the second wheel of the bogie pushes the first wheel, a high frictional force is necessary. Similar to a platform using the rocker-bogie, the use of tracks such as the FlipBot and RAPOSA requires a vertical plane and high frictional force owing to the small contact surface while climbing up [10], 11]. To resolve this issue, a few researchers from Korea combined the wheel-linkage and track mechanism into one platform [12], [13].

In addition to the rocker-bogie and track mechanism, the wheel-legged (WHEG) mechanism is used in mobile robots to overcome obstacles. For example, Rhex and ION use the WHEG mechanisms to overcome obstacles [14], [15]. Because of its curved shape, a lesser torque is required for the WHEG than for a straight leg. However, Rhex has a low climbing speed owing to control issues. It requires a separate control strategy between moving on flat ground and overcoming obstacles. However, ION is faster than Rhex because it does not have a specific control strategy. However, it is unstable when moving on a flat surface.

Besides the fixed shape mechanism, there are transforming wheel mechanisms. A passive 1-DOF mechanism is applied to a wheel transformer, land devil ray, and shape-morphing wheel [16]–[18]. Passive transformation only occurs when there is a vertical plane of the obstacle; some platforms use an active 1-DOF mechanism, and one of them uses origami to transform its wheel [19]. A robotic wheel overcomes an obstacle by pushing the spoke that forms a circular wheel [20]. FUHAR opens its spoke, which is referred to as a finger, when it climbs stairs [21]. The 1-DOF mechanism can only be used to overcome a small range of obstacle sizes. Therefore, to overcome this limitation, 2-DOF mechanisms are have been investigated. The Quattroped and STEP are examples of platforms using the 2-DOF mechanism [22], [23]. The Quattroped changes its wheel into the WHEG mechanism and moves the wheel up and down. This transformation is used to set a strategy to climb obstacles; however, using this mechanism, the Quattroped platform takes

Manuscript received February 9, 2021; accepted June 27, 2021. Date of publication July 13, 2021; date of current version December 24, 2021. This paper was recommended for publication by Editor Clement Gosselin upon evaluation of the Associate Editor and Reviewers' comments. This work was supported by Basic Science Research Program through the National Research Foundation of Korea grants funded by the Ministry of Education (NRF-2016R1D1A1B03935516 and NRF-2019R1A2C1008163). *(Corresponding authors: TaeWon Seo; Hwa Soo Kim.)*

Yunhyuk Lee, Sijun Ryu, Jee Ho Won, and TaeWon Seo are with the School of Mechanical Eng., Hanyang University, Seoul 04763, South Korea (e-mail: dldbsgur94@gmail.com; fbtlwns007@gmail.com; jhwon331@hanyang.ac.kr; taewonseo@hanyang.ac.kr).

SangGyun Kim and Hwa Soo Kim are with the Department of Mechanical System Eng., Kyonggi University, Suwon, Gyeonggi-do 16227, South Korea (e-mail: zxzx1808@naver.com; hskim94@kgu.ac.kr).

Digital Object Identifier 10.1109/LRA.2021.3096223

2377-3766 © 2021 IEEE. Personal use is permitted, but republication/redistribution requires IEEE permission.
See https://www.ieee.org/publications/rights/index.html for more information.

Authorized licensed use limited to: Northeastern University. Downloaded on March 18,2023 at 05:54:09 UTC from IEEE Xplore. Restrictions apply.

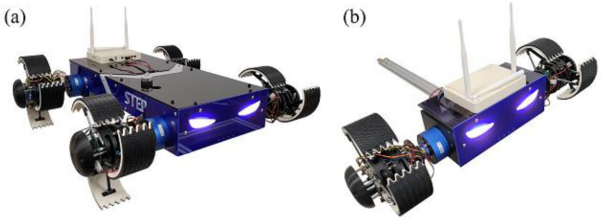

Fig. 1. A mobile platform with (a) four and (b) two modular 2-DOF transformable wheels.

a long time to overcome the obstacles. In contrast, the STEP platform transforms the wheel by changing its radius and the tilting angle of the lobe. STEP can be used to overcome various obstacle sizes by transforming its wheels even for obstacles without vertical planes. Because of the shape of the transformed wheel, it takes a short time to overcome the obstacles and is stable. The transformation of the wheel does not operate instantly because it is achieved by power transmitted far from the wheel by using a timing belt. Therefore, it is difficult to apply the wheel in other platforms.

This study presents a novel modular transformable wheel which has advantages of the 2-DOF transformable wheel and versatility. As shown in Fig. 1, different modular application designs are presented. The number of modules capable of climbing obstacles can be chosen by the designer at their desired platforms. The details of overcoming mechanism are in Section II-B. The wheel of a platform is designed as a module; therefore, the wheels can be detached and used in other platforms. Two BLDC motors are built-in, and they transform the wheel. This structure facilitates faster transformation because the rotor of the BLDC directly moves the lobe of the wheel.

The remainder of this letter is organized as follows. Section II presents the general idea of a 2-DOF transformable wheel and the 7-bar linkage mechanism to create a 2-DOF transformation. Further, the kinematic analysis and transformation range are presented. In Section III, the design and performance of the modular wheel are proposed. Experiments carried out with one modular wheel overcoming obstacles, and their results, are discussed in Section IV.

II. Two Degree of Freedom Transformable Wheel Mechanism

A. 7-Bar Mechanism for 2-DOF Transformation

The 2-DOF transformable 7-bar mechanism is shown in Fig. 2(a). One wheel consists of three wheel lobes and twelve links. There are seven links for each wheel-lobe, including the ground and wheel-lobe, as shown in Fig. 2(b). Two input links, two connecting links, and the wheel-lobe, make a 6-bar linkage. A 7-bar mechanism is created by adding one more link for the constraint of the mechanism. Seven joints are used for the 7-bar mechanism to achieve a 2-DOF transformable mechanism. As shown in Fig. 2(b), only one link is connected to a prismatic joint, whereas the other links are connected to the rotational joints.

A 2-DOF transformation is formed with two active links and four passive links. As shown in Fig. 2(b), the angle of the radius

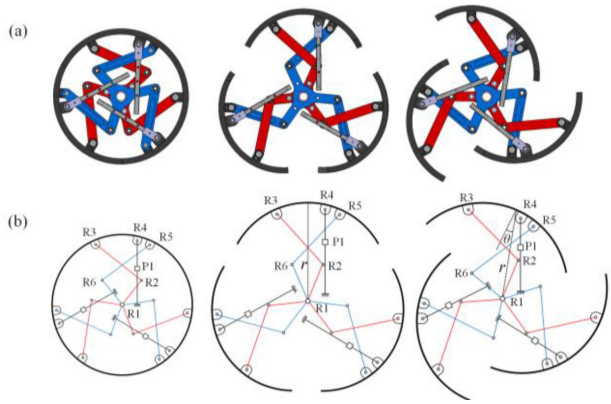

Fig. 2. 2-DOF transformable 7-bar mechanism applied to the modular wheel in (a) 3d modeling and (b) schematic diagram.

(r) of the wheel, and the angle (θ) between the center of the lobe and center of the wheel determine the shape of the transformed wheel. The two active links in the mechanism change the shape of the wheel. By rotating the two active links through the same angle, r enlarges. θ is changed by rotating the two active links at different angles. However, the two active links cannot be used to fix the position of the wheel lobe, which rotates along the active links. A link with a prismatic joint is required to prevent this rotation of the wheel-lobe.

The shape of the transformed wheel can overcome an obstacle that is at a height greater than the radius of the wheel. By changing the values of r and θ, the wheel can transform into various sizes of the WHEG. This makes it possible for the wheel to take action against different obstacle sizes. The WHEG shape can overcome obstacles stably and smoothly because it always contacts the ground using its wheel-lobe, which is arch-shaped.

B. Forward Kinematics Analysis and Jacobian Analysis

Stair is a common obstacle for service robots. In the regulation of stairs in the International Building Code (IBC), the lowest height of the riser is 102 mm [24]. Most of obstacles in indoor environment are lower than stair. Therefore, the modular wheel is designed to overcome obstacles lower than or the same as 100 mm. The length of the links in the wheel is determined to overcome the target obstacle.

Kinematic analysis is necessary to determine the workspace and singularity of the mechanism. This mechanism is similar to the parallel mechanism; therefore, a numerical method is essential to solve the forward kinematics. The Newton-Raphson method is used to determine the target value. The coordinates of all the points in Fig. 3. are expressed by the input angles. The points, lengths, and angles of the mechanism are shown in Fig. 3. Let O be the origin of the mechanism. q_1 and q_2 are the two input angles of the mechanism. l_1 to l_5 are the fixed lengths. y and φ are two output values that can determine the shape of the mechanism. y is the vertical length from p_5 to the origin. φ is the angle between l_3 and y. γ is the angle between l_3 and l_4. p_1 and p_2 can be expressed by the input angles and l_1. p_3, p_4, and p_5 are points on the wheel-lobe; they can be determined if the coordinates of one of the three points are known. The x- and

Authorized licensed use limited to: Northeastern University. Downloaded on March 18,2023 at 05:54:09 UTC from IEEE Xplore. Restrictions apply.

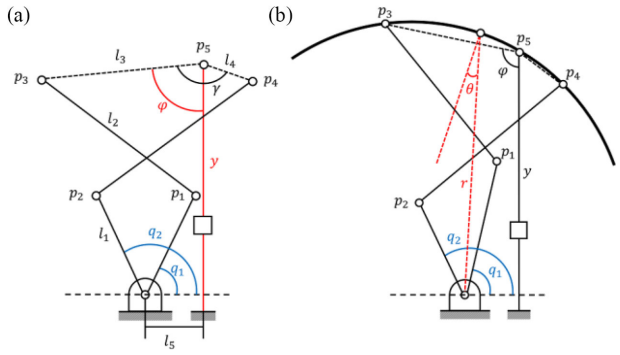

Fig. 3. Schematic diagram for forward kinematics two modular 2-DOF transformable wheels to find (a) the coordinates of all points, y and φ (b) r and θ.

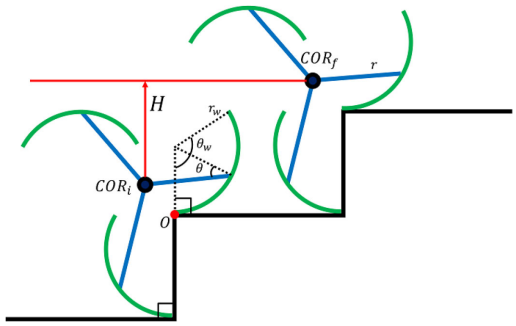

Fig. 4. Diagram to find out the height that the transformed wheel can climb where r_w is the radius of wheel-lobe and θ_w is the angle of wheel-lobe arc [23].

y-coordinates of p_5 are l_5 and y, respectively. A passive linear linkage that changes in the length of y is shifted to the right of the origin. The end effector rotates on point p_5. Therefore, the transformation depends on y and φ. The kinematic analysis is mainly performed on these two variables. From the above information p_1, p_2, p_3, and p_4 are expressed in the following manner:

$$p_1 = (l_1 \cos q_1, l_1 \sin q_1) \ , \tag{1}$$

$$p_2 = (l_1 \cos q_2, l_1 \sin q_2) \ , \tag{2}$$

$$p_3 = (l_5 - l_3 \sin \varphi, \ y - l_3 \cos \varphi) \ , \tag{3}$$

$$p_4 = (l_5 + l_4 \sin (\gamma - \varphi) , y - l_4 \cos (\gamma - \varphi)) \tag{4}$$

Because there are two unknown values, y and φ, two equations are required. These equations are obtained from two constraints on the length. The length from p_1 to p_3 and p_2 to p_4 is l_2. The function of constraint g is expressed as follows:

$$g_1 : \begin{array}{l} (l_1 \cos q_1 - \ (l_5 - l_3 \sin \varphi))^2 \\ + (l_1 \sin q_1 - (y - l_3 \cos \varphi))^2 - \ {l_2}^2 = \ 0, \end{array} \tag{5}$$

$$g_2 : \begin{array}{l} (l_1 \cos q_2 - (l_5 + l_4 \sin (\gamma - \varphi)))^2 \\ + (l_1 \sin q_2 - (y - l_4 \cos (\gamma - \varphi)))^2 - \ {l_2}^2 = \ 0, \end{array} \tag{6}$$

$$g \ (q) = \begin{bmatrix} g_1 \\ g_2 \end{bmatrix} = \begin{bmatrix} 0 \\ 0 \end{bmatrix}. \tag{7}$$

The constraint Jacobian is obtained by the time derivative of the constraint equations. Matrix G is the time derivative of the constraints. q_1 and q_2 are independent variables, and y and φ are dependent variables.

$$\frac{dg}{dt} = G \, \dot{q} = G_u \, G_v \begin{bmatrix} \dot{q}_1 \\ \dot{q}_2 \\ \dot{\varphi} \\ \dot{y} \end{bmatrix} = \begin{bmatrix} 0 \\ 0 \\ 0 \\ 0 \end{bmatrix}, \tag{8}$$

$$G_u = \begin{bmatrix} \frac{\partial g_1}{\partial q_1} & \frac{\partial g_1}{\partial q_2} \\ \frac{\partial g_2}{\partial q_1} & \frac{\partial g_2}{\partial q_2} \end{bmatrix}, \ G_v = \begin{bmatrix} \frac{\partial g_1}{\partial \varphi} & \frac{\partial g_1}{\partial y} \\ \frac{\partial g_2}{\partial \varphi} & \frac{\partial g_2}{\partial y} \end{bmatrix}. \tag{9}$$

In (9), G_u, the time derivative of the constraints about the independent variables, and G_v, about the dependent variables, are obtained from (8).

$$G_u \begin{bmatrix} \dot{q}_1 \\ \dot{q}_2 \end{bmatrix} + \ G_v \begin{bmatrix} \dot{\varphi} \\ \dot{y} \end{bmatrix} = \ 0, \tag{10}$$

$$G_v \begin{bmatrix} \dot{\varphi} \\ \dot{y} \end{bmatrix} = -G_u \begin{bmatrix} \dot{q}_1 \\ \dot{q}_2 \end{bmatrix}, \tag{11}$$

$$\begin{bmatrix} \dot{\varphi} \\ \dot{y} \end{bmatrix} = \Phi \begin{bmatrix} \dot{q}_1 \\ \dot{q}_2 \end{bmatrix}, \ \Phi = \ - G_v^{-1} \cdot G_u. \tag{12}$$

Equation (10) is a simplified form of (8). As shown in (12), Φ is the Jacobian between the independent and dependent variables.

To determine the value of each variable in the mechanism to overcome the target obstacle, a simple calculation is required. Fig. 4 shows the initial and final positions of the center of rotation (COR_i and COR_f). The initial position is when the wheel-lobe has tangential contact with the edge of the obstacle and the ground. The final position is when the wheel-lobe has tangential contact with the next obstacle. When O is the origin, the y-coordinates of the COR_i and COR_f are expressed as follows:

$$CO \ R_{iy} = r_w \ - r_w \cos\left(\frac{\theta_w}{2}\right) - r \cos\left(\pi - \theta - \frac{\theta_w}{2}\right), \tag{13}$$

$$CO \ R_{fy} = r_w \ - r_w \cos\left(\frac{\theta_w}{2}\right) + r \sin\left(\theta + \frac{\pi}{2} - \frac{\theta_w}{2}\right). \tag{14}$$

The difference between (13) and (14) is the height(H) that the wheel can overcome. H is expressed as follows:

$$\begin{aligned} H &= COR_{fy} - COR_{iy} \\ &= r \sin\left(\theta + \frac{\pi}{2} - \frac{\theta_w}{2}\right) + r\cos\left(\pi - \theta - \frac{\theta_w}{2}\right) \end{aligned} \tag{15}$$

We set one input angle to 90° and the other to 45° and changed l_1 and l_2 to determine which of them could overcome the target obstacle. The final values of each variable are listed in Table I.

Authorized licensed use limited to: Northeastern University. Downloaded on March 18,2023 at 05:54:09 UTC from IEEE Xplore. Restrictions apply.

TABLE I
VALUES OF EACH VARIABLE

Variable	l_1	l_2	l_3	l_4	l_5	l_6
Value(mm)	55	75.5	52.6	19.7	17	83

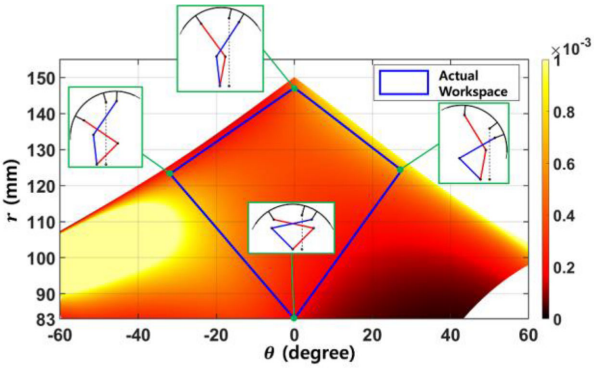

Fig. 5. The workspace and manipulability expressed by colormap and the shape of the mechanism at each corner of the actual workspace.

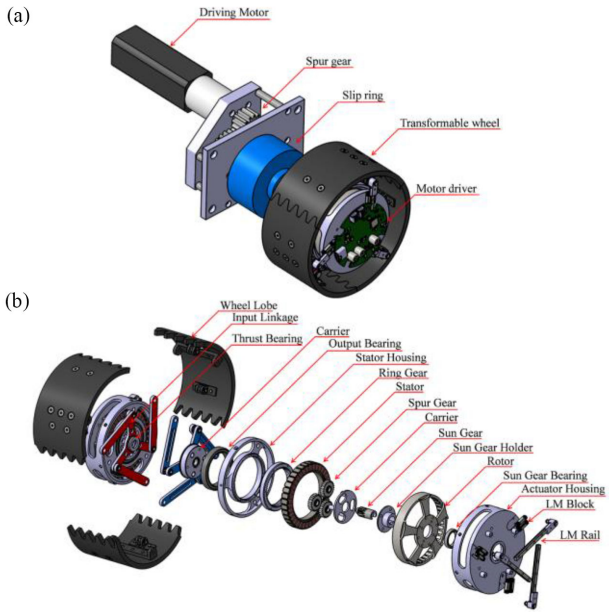

Fig. 6. Virtual model of modular wheel: (a) isometric view, (b) exploded view.

C. Transformation Range of the 2-DOF Transformation Mechanism

The workspace of the mechanism is expressed by r and θ, as shown in Fig. 5. It is obtained by changing the q_1 and q_2 ranges from 0° to 90° and 180° to 90°, respectively. There are few conditions to define the angle ranges: p_5 should be positive, the x-coordinate of p_3 should be less than p_4, and r should be larger than 83 mm because the mechanism is circular at that length. The angle θ is not symmetric with respect to the $\theta = 0°$ axis because the end effector rotates on point p_5, not the center point of the end effector. Because of this property, the position of the end effector is not symmetric when q_1 and q_2 are changed. The values of q_1 and q_2 when the wheel climbs up the obstacle should vary from when the wheel climbs down.

The manipulability (M) of the mechanism is calculated using the Jacobian matrix. The equation to determine the manipulability is as follows:

$$M = \frac{1}{cond\,(\Phi^{\mathrm{T}}\Phi)} \quad . \tag{16}$$

The value is shown in Fig. 5. The difference in manipulability is expressed by a color map. The higher the value, the better the manipulability. The lighter color indicates better manipulability than the darker color.

The actual workspace is the area inside the blue box in Fig. 5. The areas at the right and left ends make the mechanism impossible to shape. The boundary of the workspace is not included because it is close to singularity. The workspace near the blue box is not used because of the mechanical design. This will be discussed in the next section.

III. DESIGN OF THE MODULAR WHEEL

A. Mechanical Design of the Modular Wheel

The main aim of a modular design is to make the wheel applicable in any platform. A compact design is necessary for the modular design because the module is required to have all functions. There are three motors in one module: One motor is for driving the wheel, and the other two are for the transformation. The two motors for transformation are placed inside the wheel for the compact design. The characteristic of a BLDC motor is that it is available in a small compact size and provides a high torque-to-weight ratio. Therefore, BLDC motors are chosen to fit into the wheel. The driving motor is not at the same axis as the driving axis; it is shifted to one side. Otherwise, there would be a limit to the length between two modules because the driving motors of the modules would meet.

The 3D modeling of the modular wheel is shown in Fig. 6(a). The motors for transformation and driving are in one module. A slip ring is required because the power and communication cables in the wheel are rotating on a driving shaft. Two angular bearings are arranged back-to-back on the driving shaft, each of which is combined with the motor holder and plate for platform connection. Spur gears are used to transfer power to the shaft.

An expanded view of the transforming wheel is shown in Fig. 6(b). Two modified BLDC motors face each other inside the wheel. The BLDC motor has a low stall torque. To obtain a high stall torque, a gear box is installed. A planetary gear is suitable for compact design. The ring gear is installed inside the stator, and a carrier with three spur gears is placed inside the ring gear. The sun gear is combined with the sun holder and rotor of the motor. These parts form a 6:1 planetary gear inside the stator. The two housing parts are assembled with the stator and rotor.

The concentricity between the stator and rotor is a significant part of the motor; it affects the specifications of the motor. Three deep groove bearings are used for the concentricity. This type of bearing is used instead of an angular ball bearing because of its compact design. Two bearings are placed at the stator and

Authorized licensed use limited to: Northeastern University. Downloaded on March 18,2023 at 05:54:09 UTC from IEEE Xplore. Restrictions apply.

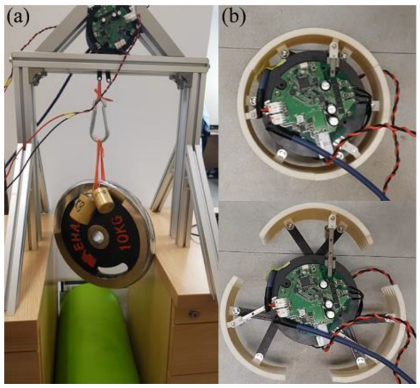

Fig. 7. Experiments to measure (a) the torque of the actuator and (b) the transformation speed.

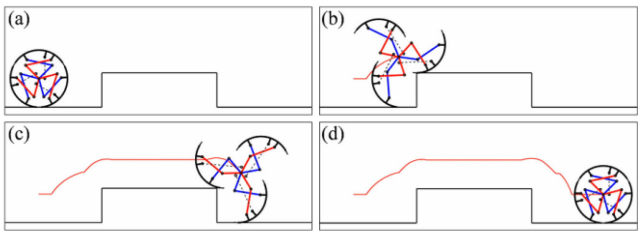

Fig. 8. The simulation of overcoming obstacle and the trajectory of the modular wheel. (a) the initial position, (b) transform to climb up 100 mm obstacle, (c) transform to climb down 100 mm obstacle, (d) transform back to circle.

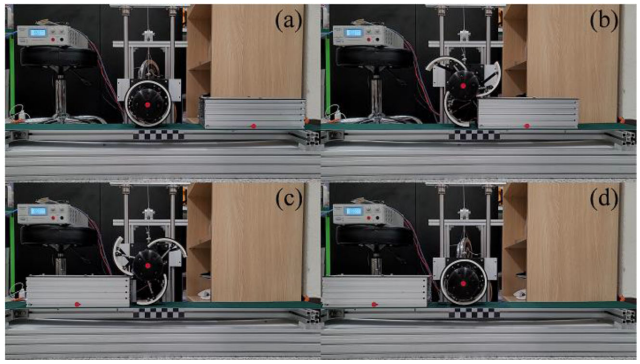

Fig. 9. The experiment of overcoming obstacle with the modular wheel. (a) the initial position, (b) transform to climb up 100 mm obstacle, (c) transform to climb down 100 mm obstacle, (d) transform back to circle.

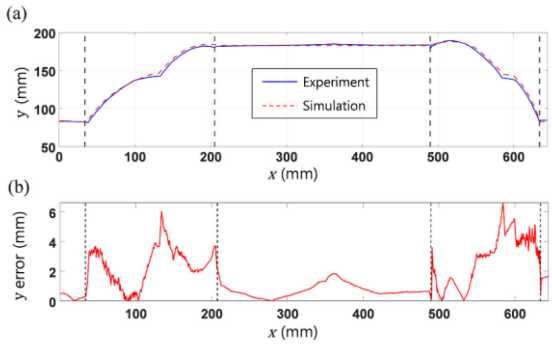

Fig. 10. (a) Comparison between trajectories between simulation and experiment (b) the rod graph showing the difference between two trajectories in y position.

actuator housing. One bearing is placed at the end of the sun gear. There is a space between the rotor and bearing at the sun gear holder. However, a spacer thicker than this is necessary to provide more preload to the bearings. This preload makes the bearings function as angular bearings.

An input linkage is attached to the carrier. The input linkage and wheel lobe are connected with one more linkage, referred to as a connecting linkage. Two input linkages are assembled face to face, and a thrust bearing is placed between them. The concentricity of the two input linkages is achieved by combining two stator housings with clinching nuts and stepped bolts. The connecting linkages of the two input linkages should move by crossing each other; thus, they must face the same side of the input linkage.

There are three wheel lobes in one modular wheel. The number of wheel lobes is three because of the contact area, stability, and transformation range. The wheel with two wheel-lobes has a large contact area; however, the center of rotation moves up and down more than the wheel with three lobes. The size of the wheel is not large; thus, four wheel lobes achieve a small range of transformation.

Three linear motion (LM) guides are attached at the actuator housing. They are shifted from the center of the wheel to secure the space for the LM rail, which is connected with the wheel lobe to obtain a prismatic joint and a constraint for the mechanism. Two input linkages, the LM guide, and the wheel-lobe form the 2-DOF transforming 7-bar mechanism.

B. Performance of the Modular Wheel

Three linear motion (LM) guides are attached at the actuator housing. They are shifted from the center of the wheel to secure the space for the LM rail, which is connected with the wheel lobe to obtain a prismatic joint and a constraint for the mechanism. Two input linkages, the LM guide, and the wheel-lobe form the 2-DOF transforming 7-bar mechanism.

The weight of the transforming wheel is 1.7 kg, and the modular wheel is 5.1 kg. The radius of the transforming wheel in the circular mode, including the thickness of the rubber sheet, is 83 mm. The torque of driving motor is 99.23 kgcm and no load speed is 82 rpm. The overall performance of the modular wheel was measured by simple experiments. The torque and transforming speed of the modular wheel were also measured. Fig. 7 shows the experimental procedure.

A torque-measuring experiment is conducted by determining the amount of mass that the actuator can lift. The initial position of the input linkage is set perpendicular to a hung mass. As shown in Fig. 7(a), the mass is tied at the input linkage, which can rotate. Consequently, one actuator can lift 11.5 kg. The length of the input linkage from the center of the actuator is 35 mm. The maximum torque is 40.25 kgcm, which is similar to 3.95 Nm.

The transforming speed is tested without any load, as shown in Fig. 7(b). The wheel starts in a circular form. The two input linkages are rotated to their maximum degree and then rotated

Authorized licensed use limited to: Northeastern University. Downloaded on March 18,2023 at 05:54:09 UTC from IEEE Xplore. Restrictions apply.

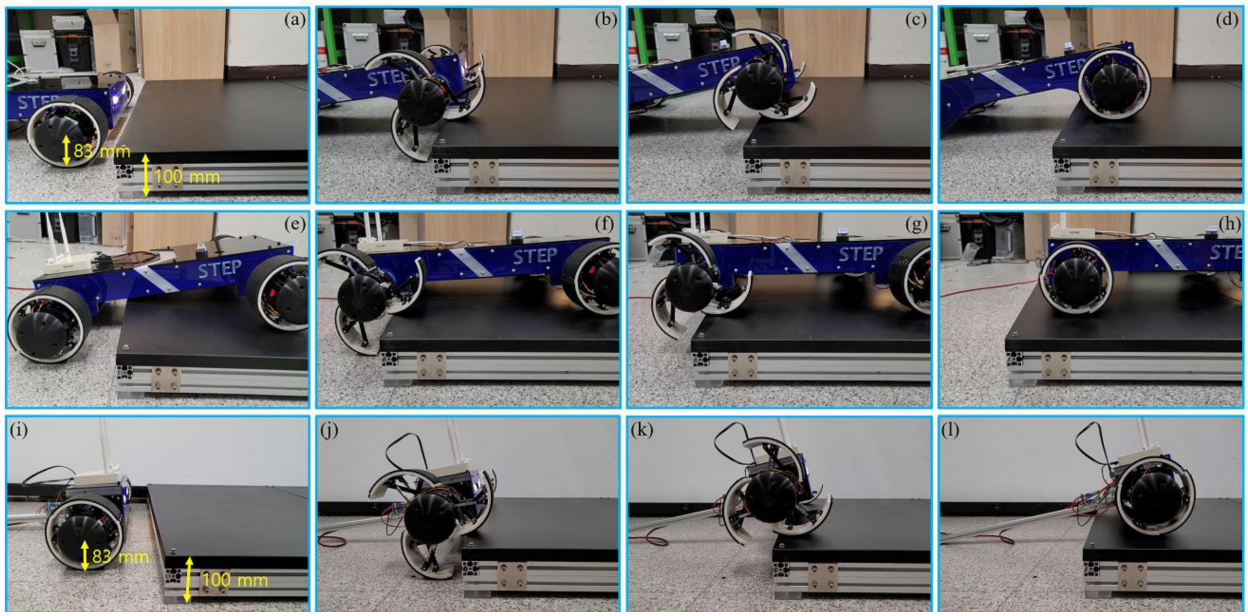

Fig. 11. Experiments with two platforms with (a)–(h) four modular wheels and (i)–(l) two modular wheels. Each platform transforms to overcome 100 mm obstacle. (a), (e) and (i) are the initial position of wheels. (b), (f) and (j) show wheels transform to WHEG form. (c), (g) and (k) show wheels start to transform to circular wheel. (d), (h) and (l) show wheels transform back to initial position.

back to the initial position. The time taken during this cycle is determined by changing the delay time between the two positions. Further, the position of each linkage is checked to determine whether it is able to follow the control. It took 500 ms to complete one cycle.

IV. Verification of Overcoming Obstacle

A. Experiment Setup for One-Wheel Experiment

A test bench was designed to conduct experiments with one modular wheel. The test bench was designed to achieve linear motion using two pipes and LM blocks. A treadmill is attached beside the two pipes so that the modular wheel can move on the treadmill. The modular wheel is fixed at the LM blocks; thus, it only moves in the vertical direction. The treadmill moves passively, and the friction of the modular wheel is the power required to move the treadmill. The modular wheel cannot transform by its own power because of the moment at the connection between the modular wheel and LM block. To verify the ability of the mechanism, external factors should be removed; a counter mass is attached to the test bench to solve this problem.

To verify the ability to overcome obstacles, an obstacle is created using aluminum profiles and an acrylic plate. The height of the obstacle is set as 100 mm to prove that the modular wheel can overcome obstacles that are higher than its radius. The riser is not included in the obstacle to prove that this mechanism can overcome the obstacle without it. The obstacle was fixed on the treadmill. Two red circular stickers, one at the center of the modular wheel, and the other at the obstacle, were used as trackers to determine the position of the center of the modular wheel. The simple planning of one wheel is achieved by simulation, as shown in Fig. 8.

B. The Result From One-Wheel Experiment

The experiment was conducted to verify the obstacle overcoming ability of the modular wheel. Similar to the simulation, the modular wheel climbed up and down the obstacle on the treadmill, as shown in Fig. 9. The rotation speed was set to a low value to enable tracking of the trajectory of the modular wheel, which is determined by tracking the center of rotation. It is measured using a MATLAB vision tracker. The red sticker at the modular wheel is used to measure the y-coordinate, and the one at the obstacle is used to measure the x-coordinate of the center of the modular wheel.

The trajectories from the simulation and experiment are shown in Fig. 10(a). The trajectory from the experiment is similar to that obtained by the simulation. The difference in the *y*-position is shown in Fig. 10(b). The sections are divided into the WHEG and circular wheel areas indicated by broken black lines. The mean difference of all sections was 1.63 mm and that of the WHEG section was 2.57 mm. It increased significantly when the modular wheel was transforming. The modular wheel in the WHEG form could not maintain its shape because of backlash from the joints and actuator. The difference at the transition point between the WHEG and circular shape is the largest. The *y-position* of the modular wheel changed significantly in an instant at the transition point.

C. Experiment with Two and Four Wheeled Platforms

The modularity of the wheel is shown using two platforms. One has four modular wheels, whereas the other has two. A 100 mm high obstacle was prepared for the experiment. Wireless communication was used to instruct the platform to transform and overcome obstacles.

Authorized licensed use limited to: Northeastern University. Downloaded on March 18,2023 at 05:54:09 UTC from IEEE Xplore. Restrictions apply.

The experiment conducted on the platform with four modular wheels is shown in Fig. 11(a)–(h). The two front modular wheels transform to the WHEG form to overcome the target obstacle. The front wheels begin to transform to the circular form immediately after the wheels climb up the obstacle. When the rear two wheels encounter the obstacle, they are transformed to the WHEG form. The rest of the process is similar to that of the front wheels overcoming the obstacle. The other experiment conducted on the platform with two modular wheels is shown in Fig. 11(i)–(l). This experiment is similar to the experiment shown in Fig. 11(a)–(h). The difference is that the two-wheeled platform has a long supporter-like tail at the rear part instead of modular wheels. The two front modular wheels transform to the WHEG form and climb the obstacle. The final position is the circular form when the platform finishes climbing the obstacle. The two platforms climb up the target obstacle with a height of 100 mm. It takes 6 seconds to climb up the obstacle: 3 seconds to transform to WHEG and climb up and 3 seconds to transform back to circular. This result shows that a modular wheel can be applied to more than one platform and overcome obstacles with a 100 mm height.

V. Conclusion

A modular 2-DOF transformable wheel was presented in this study. A 7-bar mechanism with six rotational joints and one prismatic joint was chosen for the 2-DOF transformable wheel owing to the built-in motor, as well as to facilitate fast transformation. The BLDC motor was rebuilt to insert the gear box; this built-in BLDC motor enabled the wheel to perform transformation by itself without the main body. Therefore, it was easy to assemble the main body and wheel. The performance of the modular wheel was verified using a one-wheel test bench. It was found that the modular wheel can overcome obstacles higher than its radius. Platforms with two and four modular wheels were used to demonstrate that the modular wheel can be applied to more than one platform. The ability to overcome obstacles was verified through experiments with two platforms. For future work, path planning, control and sensing issues will be applied to the platform with the modular wheel. More experiments will be conducted to verify those issues.

References

[1] "LG airstar," Accessed: May Dec., 2021. [Online]. Available: https://www.youtube.com/watch?v=7F6VZUpuMZw

[2] "Starship," Accessed: May Dec., 2021. [Online]. Available: https://www.youtube.com/watch?v=P_zRwq9c8LY

[3] "Double 2," Accessed: May Dec., 2021. [Online]. Available: https://www.youtube.com/watch?v=oI5fryQMGss

[4] "asimo," Accessed: May Dec., 2021. [Online]. Available: https://global.honda/innovation/robotics/ASIMO.html#2011

[5] "Atlas," Accessed: May Dec., 2021. [Online]. Available: https://www.youtube.com/watch?v=rVlhMGQgDkY

[6] T. Mikolajczyk, T. Fas, T. Malinowski, and L. Tomanowski, "Prototype model of walking robot," *Appl. Mechanics Mater.*, vol. 613, pp. 21–28, 2014.

[7] T. Mikolajczyk, A. Borboni, X. Kong, T. Malinowski, and A. Olaru, "3D printed biped walking robot," *Appl. Mechanics Mater.*, vol. 772, pp. 477–481, 2015.

[8] R. Siegwart, P. Lamon, T. Estier, M. Lauria, and R. Piguet, "An innovative design for wheeled locomotion in rough terrain," *Robot. Auton. Syst.*, vol. 40, no. 2/3, pp. 151–162, 2002.

[9] T. Thueer, P. Lamon, A. Krebs, and R. Seigwart, "Crab – exploration rover with advanced obstacle negotiation capabilities," in *Proc. 9th ESA Workshop Adv. Space Technol. Robot. Automat.*, 2006, pp. 28–30.

[10] B. Seo, H. Kim, M. Kim, K. Jeong, and T. Seo, "FlipBot: A new field robotic platform for fast stair climbing," *Int. J. Precis. Eng. Manuf.*, vol. 14, no. 11, pp. 1909–1914, 2013.

[11] C. Marques, J. Cristovao, P. Lima, J. Frazao, I. Ribeiro, and R. Ventura, "RAPOSA: Semi-autonomous robot for rescue operations," in *Proc. EEE/RSJ Int. Conf. Intell. Robots Syst.*, 2006, pp. 3988–3993.

[12] D. Choi, Y. Kim, S. Jung, J. Kim, and H. S. Kim, "A new mobile platform (RHyMo) for smooth movement on rugged terrain," *IEEE/ASME Trans. Mechatronics*, vol. 21, no. 3, pp. 1302–1314, Jun. 2016.

[13] D. Choi, J. R. Kim, S. Cho, S. Jung, and J. Kim, "Rocker-Pillar: Design of the rough terrain mobile robot platform with caterpillar tracks and rocker bogie mechanism," in *Proc. IEEE/RSJ Int. Conf. Intell. Robot. Syst.*, 2012, pp. 3405–3410.

[14] U. Saranli, M. Buehler, and D. E. Koditschek, "RHex:Asimple and highly mobile hexapod robot," *Int. J. Robot. Res.*, vol. 20, no. 7, pp. 616–631, 2001.

[15] S. P. Agrawal, H. Dagale, N. Mohan, and L. Umanand, "IONS: A quadruped robot for multi-terrain applications," *Int. J. Mater., Mechanics Manuf.*, vol. 4, no. 1, pp. 84–88, 2016.

[16] Y. Kim, G. Jung, H. Kim, K. Cho, and C. Chu, "Wheel transformer: A miniaturized terrain adaptive robot with passively transformed wheels," in *Proc. Int. Conf. Robot. Automat.*, 2013, pp. 5625–5630.

[17] L. Bai, J. Guan, X. Chen, J. Hou, and W. Duan, "An optional passive/active transformable wheel-legged mobility concept for search and rescue robots," *Robot. Auton. Syst.*, vol. 107, pp. 145–155, 2018.

[18] S. Ryu, Y. Lee, and T. Seo, "Shape-morphing wheel design and analysis for step climbing in high speed locomotion," *IEEE Robot. Automat. Lett.*, vol. 5, no. 2, pp. 1977–1982, Apr. 2020.

[19] D. Lee, S. Kim, J. Kim, J. Park, and K. Cho, "Origami wheel transformer: A variable-diameter wheel drive robot using an origami structure," *Soft Robot.*, vol. 4, no. 2, pp. 163–180, 2017.

[20] N. Moriya, H. Shigemune, and H. Sawada, "A robotic wheel locally transforming the diameter for the locomotion on rough terrain," in *Proc. IEEE Int. Conf. Mechatronics Automat.*, 2020, pp. 1257–1262.

[21] İ. Mertyüz, A. K. Tanyıldızı, B. Taşar, A. B. Tatar, and O. Yakut, "FUHAR: A transformable wheel-legged hybrid mobile robot," *Robot. Auton. Syst.*, vol. 133, pp. 103627, 2020.

[22] S. Chen, K. Huang, W. Chen, S. Shen, C. Li, and P. Lin, "Quattroped: A leg-wheel transformable robot," *IEEE/ASME Trans. Mechatronics*, vol. 19, no. 2, pp. 730–742, Apr. 2014.

[23] Y. Kim, Y. Lee, S. Lee, J. Kim, H. S. Kim, and T. Seo, "STEP: A new mobile platform with 2-DOF transformable wheels for service robots," *IEEE/ASME Trans. Mechatronics*, vol. 25, no. 4, pp. 1859–1868, Aug. 2020.

[24] "International building code 2009," Accessed: May Dec., 2021. [Online]. Available: https://up.codes/viewer/alabama/ibc-2009/chapter/10/means-of-egress#1009.4.2

Authorized licensed use limited to: Northeastern University. Downloaded on March 18,2023 at 05:54:09 UTC from IEEE Xplore. Restrictions apply.